even though Io's plasma environment shows large variations. This suggests the existence of some protected reservoir. The calculations above show that the lifetime of the inventory in the range $\sim 1\ r_{Io}$ to $10\ r_{Io}$ is too short to perform that function. The surface itself or a dense atmosphere inside $1.4\ r_{Io}$ may be acting as a buffer.

REFERENCES AND NOTES

1. A review of our current understanding of Io and the major unresolved questions appears in several chapters of *Satellites*, J. A. Burns and M. S. Matthews, Eds. (Univ. of Arizona Press, Tucson, 1986).
2. The sputtering process involves the impact of high-energy ions on a surface or thick atmosphere, and the subsequent release and ejection of high-speed atoms and molecules over a range of velocities. See the review by A. F. Cheng, P. K. Haff, R. E. Johnson, and L. J. Lanzerotti in (*1*), p. 403. This chapter also includes estimates of the supply rates to the torus and neutral clouds.
3. The emission was discovered by R. A. Brown [in *Exploration of the Planetary System*, A. Woszczyk and C. Iwaniszewska, Eds. (Reidel, Dordrecht, 1974), p. 527]. L. Trafton, T. Parkinson, and W. Macy [*Astrophys. J.* **190**, L85 (1974)] determined that the emission came from an extended region around Io.
4. B. A. Goldberg *et al.*, *Science* **226**, 512 (1984).
5. R. A. Brown, R. M. Goody, F. J. Murcray, *Astrophys. J.* **200**, L49 (1975).
6. Five eclipses were successfully observed, but we discuss only two. Eclipse 1 was only grazing: Europa slowly approached Io's shadow from the east, barely touched it, and then receded again to the east. Eclipse 2 was deep but fast: Europa passed rapidly through the shadow from west to east. Favorable eclipses were also observed on 15, 21, and 23 September 1985 (see N. M. Schneider, thesis, University of Arizona, in preparation). The eclipse series occur every 6 years [K. Aksnes and F. Franklin, *Icarus* **60**, 180 (1984); and J. E. Arlot, *Astron. Astrophys.* **138**, 113 (1984)].
7. The term impact parameter is defined as the perpendicular distance between the incident solar beam of light and Io's center.
8. The Catalina Observatory data are spatially resolved CCD (charge-coupled device) spectra with Io and Europa simultaneously recorded. The rows spanning Europa's spectrum were weighted according to noise and summed for collapse to one dimension. Terrestrial water lines were removed by means of the spectrum of a rapidly rotating B-star, and the solar lines were eliminated by dividing by a similarly corrected spectrum of Europa far from eclipse. Equivalent widths were measured digitally by summing over the absorption feature. The primary error stems from the subjective placement of the continuum. Error bars are estimated 90% confidence intervals.
9. The McDonald Observatory data are one-dimensional spectra of Europa. The solar and telluric lines were removed with a combination of lunar and Ganymede spectra. Equivalent widths were determined by approximating the absorption feature by a triangle and measuring the area relative to the continuum. A subset of the simultaneous Catalina Observatory data was reduced, and the results were used in the final determination of the error bars.
10. The equivalent width W is defined as the integral over the normalized spectrum of the difference between the continuum and the absorption feature. The result is in units of wavelength, in this case milliangstroms (mÅ). It is the width of a completely saturated absorption feature whose W matches the observed line.
11. E. M. Sieveka and R. E. Johnson, *Astrophys. J.* **287**, 418 (1984).
12. J. H. Lieske of the Jet Propulsion Laboratory provided the ephemeris listing of satellite positions corrected for light-time. These positions were input to an eclipse-simulating program that calculated the apparent center of light of Europa during eclipse.
13. L. Trafton and W. Macy, *Icarus* **33**, 322 (1978).
14. Summers *et al.* constructed a Chamberlain-type exosphere similar to the one used here (M. E. Summers, D. F. Strobel, Y. L. Yung, J. T. Trauger, F. Mills, in preparation). M. A. McGrath and R. E. Johnson [*Icarus* **69**, 519 (1987)] generated a corona around Io by modeling the ballistic trajectories of atoms and molecules ejected by sputtering from the exobase.
15. The exobase is defined as the location from which a high-speed atom has a $1/e$ chance of escaping without colliding with another atom. Using a typical collision cross section $\sigma = 30$ Å^2, we calculate the appropriate integrated density $1/\sigma = 3 \times 10^{14}$ cm^{-2}.
16. Only two measurements of the sodium mixing ratio near Io have been made, both involving Voyager ion experiments. The upper limit of sodium in the cold torus plasma is estimated at $\leq 5\%$ [F. Bagenal and J. D. Sullivan, *J. Geophys. Res.* **86**, 8447 (1981)]. N. Gehrels and E. Stone [*ibid.* **88**, 5537 (1983)] measured a 3% sodium mixing ratio with the low-energy telescope experiment. One effect that can reduce neutral sodium's local mixing ratio is its short lifetime against ionization; sodium at a distance of several r_{Io} could be depleted by up to a factor of 10 compared to other constituents.
17. In a charge-exchange reaction, a high-speed (~ 57 km sec^{-1}) sodium ion accepts an electron from a sodium atom, thereby becoming a fast neutral. The cross section for this reaction is ~ 150 Å^2. Jets of these neutrals have been reported by J. T. Trauger [*Bull. Am. Astron. Soc.* **16**, 712 (1984) (abstr.)] and N. M. Schneider, D. M. Hunten, and R. A. Brown [*ibid.* (abstr.), p.663].

18. We thank U. Fink, A. B. Schultz, and M. A. DiSanti for providing and operating the CCD camera for the Lunar and Planetary Laboratory echelle spectrograph; J. H. Lieske, F. A. Franklin, and K. Aksnes for ephemeris calculations; R. A. Tucker for observing assistance; and R. L. Marcialis, J. R. Spencer, and E. Karkoshka for photometric support. R. V. Yelle provided the exospheric calculations. N.M.S., D.M.H., and W.K.W. acknowledge the support of NASA grant NAGW-596 and L.M.T. acknowledges NASA grant NGR44-012-152. The CCD is operated under NASA grant NSG 7070. We thank R. A. Brown, W. H. Smyth, and M. E. Summers for helpful discussions, and E. Ellingson for drawing our attention to the eclipses in the first place.

27 February 1987; accepted 7 July 1987

Electromagnetic Stabilization of Weakly Conducting Fluids

CORNELIUS F. IVORY,*† WILLIAM A. GOBIE, JAMES B. BECKWITH, ROBERT HERGENROTHER, MICHAEL MALEC

Classical hydromagnetic theory predicts that the flow of dilute aqueous electrolyte in a slit can be stabilized by application of a strong, transverse magnetic field. However, recent experiments indicate that stabilization can be achieved with the use of a much weaker field in the presence of a small lateral current. A revised theory describes how the magnetic and electric fields interact to eliminate natural convection.

WHEN A HORIZONTAL LIQUID film is heated uniformly from below, a patterned flow consisting of spatially periodic rolls or cells (Fig. 1) may develop if the temperature gradient, ∇T, causes the Rayleigh number

$$Ra \equiv \frac{\rho g \beta |\nabla T| h^4}{\eta \kappa} \quad (1)$$

to exceed its critical value. In this expression $\rho(T)$ is the density, g is the gravitational acceleration, β is a thermal expansion coefficient, h is the thickness of the film, η is the viscosity, and κ is the thermal diffusivity of the fluid. For a horizontal slit bounded by perfectly conducting walls this critical value is $Ra_c \approx 1708$ (*1*).

A related instability occurs if the slit is oriented vertically while maintaining the temperature gradient parallel to gravity. For example, consider a chamber (Fig. 2) in which a thin film of electrolyte is heated by an electric current. In this case experiments conducted at Ra slightly higher than the

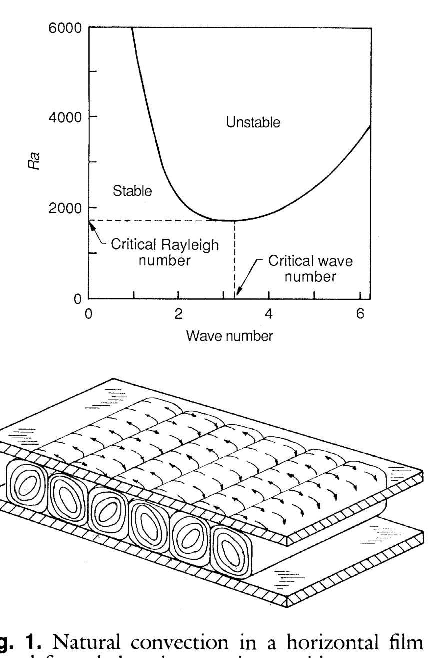

Fig. 1. Natural convection in a horizontal film heated from below is sometimes evident as spatially periodic rolls or cells. Convection may occur when the Rayleigh number exceeds its critical value, in this case $Ra_c \approx 1708$.

Department of Chemical Engineering, University of Notre Dame, Notre Dame, IN 46556.

*To whom correspondence should be addressed.
†Present address: Department of Chemical Engineering, Washington State University, Pullman, WA 99164.

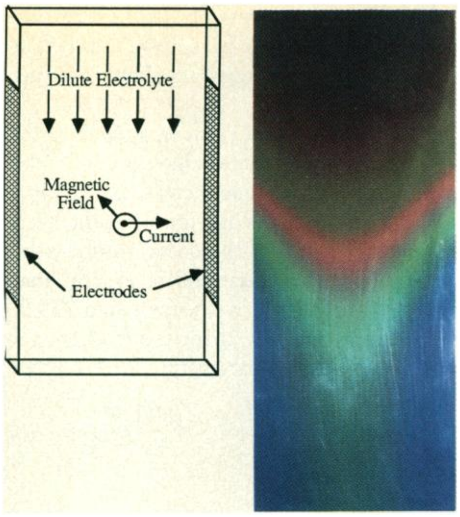

Fig. 2. (**Left**) Schematic of the electrically heated vertical slit. Current is directed laterally between the electrodes and fluid flows parallel to gravity. The temperature increases axially as a result of Joule heating as the fluid flows through the slit. The transverse axis crosses the thin dimension of the slit. (**Right**) Observed temperature profile on the rear surface of an insulated slit with stable flow. The color code on the liquid crystal thermometer mounted on the rear surface of the slit is 74°F, black; 75°F, red; 76°F, green; 77°F, blue; and 78°F, black. The incoming temperature is approximately 74°F and the exit temperature is just below 78°F.

critical value produce stationary flow cells which may appear in either symmetric or antisymmetric patterns when viewed through the transverse surfaces and which tend to periodic and apparently aperiodic behavior as *Ra* is increased. This type of behavior has been predicted (*2*) and observed (*3*) in jacketed chambers and has recently been observed (Fig. 3) in insulated chambers.

According to classical hydromagnetic theory (*1, 4*), a thermally destabilized flow of aqueous electrolyte in a vertical slit can be stabilized by applying a magnetic field of 10^2 to 10^3 kG through the transverse face of the slit. However, our experiments with insulated slits indicate that weakly conductive electrolytes, ~10 m*M* NaCl, supporting a small lateral electric field, 10 V/cm for instance, can be stabilized by a 1-kG field. Stabilization occurs because of an extraordinary coupling between the transverse magnetic field and axial gradients in the current. As electrolyte flows through the slit, it is warmed by Joule heating, and, as its temperature increases, its conductivity increases slightly so that a little more current is conducted laterally across the slit at points farther down the column. This slight excess current, $\delta\mathbf{I}$, couples with the applied magnetic field, $\mathbf{B}$, to exert a differential force on the fluid, $(\delta\mathbf{I})\times\mathbf{B}$, which can either counteract or enhance the excess buoyancy term, $(\delta\rho)\mathbf{g}$.

This coupling allows one to set the magnetic field so that it offsets the buoyancy force by adjusting the magnitude and direction of the field until these forces cancel. Since the driving force for natural convection can be counteracted in this manner, it is possible to damp both stable and unstable convection in the slit. Furthermore, if the magnetic field is reversed, the Lorentz force will supplement the buoyancy force and reinforce the thermally induced convection.

This effect may find practical application in the stabilization or destabilization of slit flows in specialized heat exchangers, electrolytic cells, or free-flow electrophoresis equipment. Furthermore, it may allow terrestrial simulation of extraterrestrial experiments by balancing out the effect of gravity. However, it is not necessary to rely on the presence of naturally occurring gradients in the conductivity; one may generate the gradient by purely artificial means and apply either steady or modulated fields to stabilize or destabilize the system (*5*).

The apparatus used in these experiments consists of two rectangular blocks (14 by 60 by 3 cm^3) of Plexiglas, which, when bolted together, form a 2-mm-thick slit. The front surface of the slit is transparent, and the back face is fitted with a thin sheet of Teflon bonded to a steel plate. The white Teflon surface provides an excellent backdrop for flow visualization studies while a liquid crystal thermometer mounted on the back side of the plate displays the approximate temperature profile in the slit. To provide the current, platinum wire electrodes 7.5 cm long are mounted on each end of the slit and continuously flushed with buffered electrolyte to remove the products of electrolysis. During the experiments buffered saltwater is introduced by gravity feed into a header located at the top of the chamber. It flows 17.8 cm through the slit before reaching a 7.6-cm-long electrode section and another 17.8 cm after the electrode section before exiting the chamber. Five dye streaks are introduced near the top of the slit to allow visualization of the flow.

A small laboratory magnet with a 7.5-cm adjustable gap and 10-cm-diameter poles is mounted on a cart so that it can be withdrawn from the chamber when the magnetic field is switched off. The magnet is initially situated over the chamber so that it straddles the electrode section while the poles face through the transverse Plexiglas surfaces. With the poles fully separated, it is possible to directly observe the effect of the magnetic field on the streamlines.

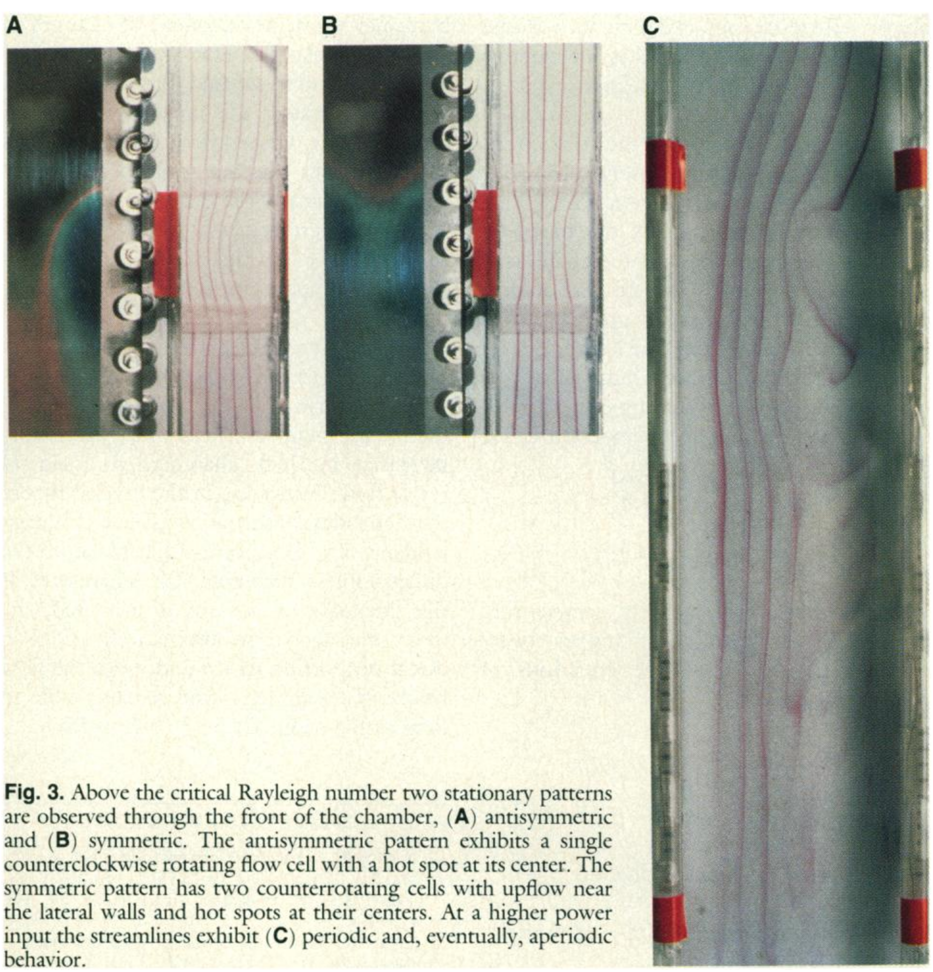

Fig. 3. Above the critical Rayleigh number two stationary patterns are observed through the front of the chamber, (**A**) antisymmetric and (**B**) symmetric. The antisymmetric pattern exhibits a single counterclockwise rotating flow cell with a hot spot at its center. The symmetric pattern has two counterrotating cells with upflow near the lateral walls and hot spots at their centers. At a higher power input the streamlines exhibit (**C**) periodic and, eventually, aperiodic behavior.

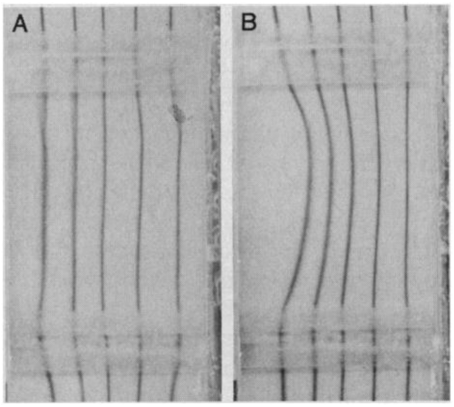

Fig. 4. Less than 2 seconds after the magnet has been removed from the chamber the flow is still stable (**A**) but may exhibit bowing as a result of electrode end effects. This can be minimized by carefully adjusting the magnetic field as was done for this photo. Note the imminent breakdown of the stabilized flow at the top of the picture shortly after the magnetic field has been turned off. Several minutes later the flow reverts to an unstable pattern (**B**).

In the absence of a magnetic field the least stable secondary mode is predicted to be antisymmetric (*2*), as illustrated by the temperature and flow patterns in Fig. 3A. If Ra is raised slightly, either by increasing the power input or by decreasing the flow rate, the symmetric patterns illustrated in Fig. 3B sometimes appear. In most of our experiments the two flow patterns appear under virtually indistinguishable conditions. At higher Ra the flow exhibits periodic behavior (Fig. 3C).

When the magnetic field is turned on, the strength of the induced flow either increases or decreases, depending on the direction of the field. For instance, the flow cells can be entirely eliminated by correctly adjusting the strength and direction of the magnetic field (Fig. 4). Oscillations may be induced from either of the stationary flow patterns with the magnetic field oriented in one direction or damped if the field is reversed.

The velocity, $\mathbf{v}$, of a conductive fluid in the presence of magnetic and electric fields is described by the Navier-Stokes equation, which includes a term for the Lorentz force

$$\rho \frac{\partial \mathbf{v}}{\partial t} + \rho \mathbf{v} \cdot \nabla \mathbf{v} = -\nabla p + \eta \nabla^2 \mathbf{v} + \rho \mathbf{g} + \mathbf{I} \times \mathbf{B} \tag{2}$$

where p is the pressure. This equation is simplified by expanding the density in a Taylor series in the temperature from which the higher order terms are truncated

$$\rho(T) = \rho(T_0) + \left(\frac{d\rho}{dT}\right)_{T=T_0} (T - T_0) + \ldots$$
$$\approx \rho(T_0) - \rho\beta(T - T_0) \tag{3}$$

combining it with the equations of conservation of mass and thermal energy and then invoking the Boussinesq approximation (*1*).

In classical hydromagnetic theory (*4*) these equations are further combined with Maxwell's equations of electromagnetism and solved by linear stability analysis. For a slit with perfectly conducting transverse surfaces this yields a critical Rayleigh number that increases with the square of the magnetic field strength,

$$Ra_c = \pi^4 + \pi^2 M^2 \tag{4}$$

where the effect of the magnetic field is characterized by the Hartmann number, M, defined as

$$M^2 \equiv \frac{\sigma B^2 h^2}{\rho \nu} \tag{5}$$

where σ is the electrical conductivity. In the absence of a magnetic field, $M = 0$ so that the critical parameter is $Ra_c \approx 97.41$ in the vertical slit (*2, 6*), substantially lower than its horizontal counterpart.

According to classical theory, a magnetic field applied across the slit will always act to damp secondary flows, regardless of the direction of the field, since it always increases Ra_c. This theory also predicts that a magnetic field greater than 100 kG is required to generate a Hartmann number of 1.0 in a 2-mm slit under the conditions cited above. However, our experiments indicate that a field strength of 1 kG is sufficient to stabilize the flow if the magnetic field is correctly oriented.

The differences between the predictions of classical theory and the observed behavior are readily explained in a revised theory that ignores currents induced by the magnetic field but takes into account the small axial gradients in the lateral current that accompany the axial temperature gradient. This effect is incorporated into the Navier-Stokes equations by substituting Ohm's law, $\mathbf{I} = \sigma \mathbf{E}$, for the current, expanding σ in a Taylor series around the reference temperature, T_0,

$$\sigma(T) = \sigma(T_0) + \left(\frac{d\sigma}{dT}\right)_{T=T_0} (T - T_0) + \ldots$$
$$\approx \sigma(T_0) + \sigma\gamma(T - T_0) \tag{6}$$

where γ is the conductivity temperature coefficient, and truncating higher order terms. On substitution the equations of motion become

$$\rho \frac{\partial \mathbf{v}}{\partial t} + \rho \mathbf{v} \cdot \nabla \mathbf{v} = -\nabla P + \eta \nabla^2 \mathbf{v}$$
$$- \rho\beta(T - T_0)\mathbf{g} - \sigma\gamma(T - T_0)\mathbf{E} \times \mathbf{B} \tag{7}$$

where P is the augmented pressure,

$$P \equiv p + \rho g x - \sigma \mathbf{E} \times \mathbf{B} \cdot [x\mathbf{i} + y\mathbf{j} + z\mathbf{k}] \tag{8}$$

The last two terms in this expression contribute only to the base flow, and the last term, in particular, causes a slight bending of the flow.

The buoyancy and electromagnetic terms in the equation of motion have precisely the same temperature dependence, and, if they are added together while ignoring the nonaxial components of the cross product, the structure of the equations is exactly that obtained from classical theory when $M = 0$. Using linear stability theory, one obtains a new dimensionless parameter

$$N \equiv \frac{\rho g \beta |\nabla T| h^4}{\eta \kappa} + \frac{\gamma I B |\nabla T| h^4}{\eta \kappa} \tag{9}$$

with the critical value

$$N_c = \pi^4 \tag{10}$$

The first term on the right in Eq. 9 is Ra and the second term accounts for the excess Lorentz force. By adjusting the directions of $\mathbf{I}$ and $\mathbf{B}$, the second term in Eq. 9 may be made negative to reduce N below its critical value or positive to destabilize the flow.

Comparing the two dimensionless terms in Eq. 9, we see that when

$$\left| \frac{\sigma\gamma E B}{\rho g \beta} \right| > 1 \tag{11}$$

the electromagnetic term dominates the buoyancy term, independent of changes in the slit thickness. For water, the ratio $\gamma/\beta \approx 250$ and so we find that roughly 1 kG is needed to satisfy this inequality and guarantee stability. Under these same conditions the Hartmann number squared is roughly $M^2 \approx 10^{-5}$ and so the magnetic field would need to be increased by at least two orders of magnitude before this term could have a significant impact on hydrodynamic stability.

Since M^2 increases with the second power of the chamber thickness while Ra increases with the fourth power, according to classical theory the magnetic field must be sharply increased in thick chambers to maintain stable flow. However, in the revised theory the dependence on the transverse thickness is identical in both terms that make up the dimensionless parameter N. Therefore, as the thickness of the slit is increased, the electromagnetic term automatically grows in direct proportion to Ra and, once the flow has been stabilized, it will remain stable so long as the magnetic field remains fixed.

REFERENCES AND NOTES

1. S. Chandrasekhar, *Hydrodynamic and Hydromagnetic Stability* (Dover, New York, 1961), pp. 9–71 and 146–154; J. A. Whitehead, Jr., *Am. Sci.* **59**, 444 (1971).
2. D. A. Saville and S. Ostrach, *Fluid Mechanics of Continuous Flow Electrophoresis*, Final Report on

Contract NAS8-31349 Code 361 (Princeton University, Princeton, NJ, 1978), pp. 60–67; D. A. Saville, *Physicochem. Hydrodyn.* 1, 297 (1980); in *Physicochemical Hydrodynamics, V. G. Levich Festschrift*, B. D. Spaulding, Ed. (Advance Publications, London, 1977), pp. 907–910.
3. P. H. Rhodes and R. S. Snyder, in *Materials Processing in the Reduced Gravity Environment of Space*, vol. 9 of *Materials Research Society Symposia Series*, G. E. Rindone, Ed. (Elsevier, Amsterdam, 1982), pp. 225–233.
4. N. T. Dunwoody, *J. Fluid Mech.* **20**, 103 (1964); R. C. Lock, *Proc. R. Soc. London Ser. A* **233**, 105 (1955).
5. A. Kolin, D. Leenov, W. Lichten, *Biochim. Biophys. Acta* **32**, 538 (1959); A. Kolin, in *Electrokinetic Separation Methods*, P. G. Righetti *et al.*, Eds. (Elsevier/North-Holland, Amsterdam, 1979), pp. 169–172.
6. R. A. Wooding, *J. Fluid Mech.* **7**, 501 (1960); G. I. Taylor, *Z. Angew. Math. Mech.* **13**, 147 (1933).
7. The material presented in this report is based on work supported in part under NSF grant CBT-8414218.

29 April 1987; accepted 30 June 1987

X-ray Photographs of a Solar Active Region with a Multilayer Telescope at Normal Incidence

J. H. Underwood, M. E. Bruner, B. M. Haisch, W. A. Brown, L. W. Acton

An astronomical photograph was obtained with a multilayer x-ray telescope. A 4-centimeter tungsten-carbon multilayer mirror was flown as part of an experimental solar rocket payload, and successful images were taken of the sun at normal incidence at a wavelength of 44 angstroms. Coronal Si-XII emission from an active region was recorded on film; as expected, the structure is very similar to that observed at O-VIII wavelengths by the Solar Maximum Mission flat crystal spectrometer at the same time. The small, simple optical system used in this experiment appears to have achieved a resolution of 5 to 10 arc seconds.

Significant recent advances in x-ray optics, spurred in part by new astronomical applications, include the development of thin-film, layered synthetic microstructures (multilayers) to achieve x-ray and extreme ultraviolet reflection at normal incidence (*1*). This can in principle be achieved down to a wavelength of $\lambda \approx 20$ Å, limited by the atomic dimensions of individual dielectric–spacer pair monolayers, and with reflectivity $R \approx 0.5$, over a passband, $\Delta\lambda/\lambda \approx 0.01$. This technology is of considerable interest to x-ray astronomers (*2, 3*). For a given mirror aperture a normal incidence imaging system with multilayer mirrors has an enormous advantage over grazing incidence systems in effective area and field-of-view. In addition, the surfaces are much simpler than the steep conic sections of grazing incidence optics and are therefore much easier to figure to a high degree of accuracy. Moreover, the narrowness of the passband can be used to isolate individual spectral lines and thereby make images of specific temperature regimes. Although laboratory imaging experiments have been successful in the past (*4*), to the best of our knowledge no astronomical object had been imaged with a multilayer reflector. Figure 1 is an image of a solar active region taken with a multilayer telescope.

J. H. Underwood, Lawrence Berkeley Laboratory, Berkeley, CA 94720.
M. E. Bruner, B. M. Haisch, W. A. Brown, L. W. Acton, Lockheed Palo Alto Research Laboratory, Palo Alto, CA 94304.

The x-ray mirror was prepared by the Energy Conversion Devices Corporation. By means of a sputtering technique, 30 tungsten-carbon layer pairs (nominally 7.65 Å of tungsten and 14.5 Å of carbon) were deposited on a 4-cm-diameter spherical mirror having a 2-m concave radius of curvature. The mirror was designed for imaging the strong Si-XII line pair at 44.16 and 44.02 Å, slightly to the long wavelength side of the carbon K absorption edge (43.68 Å); this considerably simplified the filtering out of shorter wavelength x-ray lines. The multilayer diffraction plane-spacing was measured to be 21.93 Å on the basis of the angular reflection peak of a monochromatic beam. The mirror was designed to have a relatively broad band, hence a moderate peak reflectivity, $R \approx 0.025$. The peak wavelength of 43.86 Å met the design requirement; the absolute value of R has not yet been verified experimentally.

Figure 2 shows the Si-XII lines in relation to other solar emission features in this spectral region; the comparison spectrum was taken during a solar flare by a Lockheed rocket-borne spectrograph on 13 July 1982 (*5*). Si-XII radiation is emitted by coronal plasma at $T \approx 1.5 \times 10^6$ to 4×10^6 K, typical of active region loops, although the tail of the emissivity curve can extend to flare-like temperatures above 10^7 K (*6*). Second-order lines of O VII ($\lambda_{true} \approx 22$ Å) and third-order lines of Fe XVII ($\lambda_{true} \approx 15$ Å) are also present (dotted in the figure),

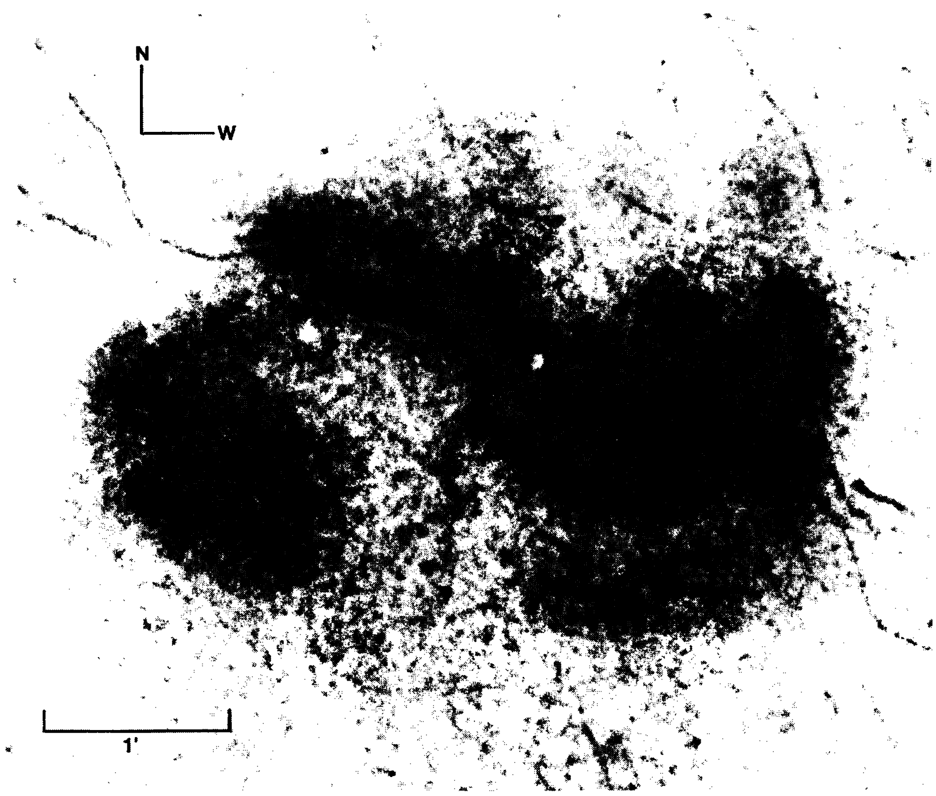

Fig. 1. A soft x-ray image of solar active region 4698/99 as imaged by a 4-cm diameter, *f*/20, multilayer telescope at a wavelength of 44 Å.